Polym. Bull. (2016) 73:1207–1227
DOI 10.1007/s00289-015-1543-9

ORIGINAL PAPER

Development of long-term antimicrobial poly (ε-caprolactone)/silver exchanged montmorillonite nanocomposite films with silver ion release property for active packaging use

Fayçal Benhacine[1] · Assia siham Hadj-Hamou[1] · Abderrahmane Habi[2]

Received: 7 February 2015 / Revised: 16 September 2015 / Accepted: 23 October 2015 /
Published online: 30 October 2015

Abstract Poly (ε-caprolactone)/silver exchanged montmorillonite (PCL/Ag–MMT) nanocomposites with a strong antibacterial activity and a slow release property were successfully prepared via solvent casting method, for active packaging use. The PCL/Ag–MMT nanocomposites containing different Ag–MMT loadings were characterized by several techniques. X-Ray Diffraction (XRD), UV–visible Spectroscopy and Transmission Electron Microscopy (TEM) results revealed that the MMT layers were exfoliated and spherical Ag nanoparticles were randomly distributed in the polymer matrix. Differential scanning calorimetry (DSC) showed that glass transition and melting temperatures of PCL/Ag–MMT nanocomposites were unaffected by clay contents compared to neat PCL. Nevertheless, the crystallization temperatures were increased due to the incorporation of effective nucleation agent Ag–MMT and its satisfactory dispersion into the PCL matrix. The positive effect of the Ag–MMT addition on the PCL barrier properties was confirmed by the reduction in the water permeability (WVP). Tensile results also displayed an improvement of mechanical properties for the PCL/Ag–MMT nanocomposites due to the insertion of clay particles into the PCL matrix. The potential of the silver ion release from the PCL/Ag–MMT films to a slightly acidified water medium was measured by atomic absorption spectroscopy. The results exhibited a gradual increase of the amount of silver ions released up to 30 days of immersion. The kinetic study of the ions release showed that the release's mechanism is governed by the diffusion process. The apparent diffusivity

✉ Assia siham Hadj-Hamou
hadjhamouassia@yahoo.fr

[1] Laboratoire des Matériaux Polymères, Département de chimie macromoléculaire, Faculté de Chimie, Université des Sciences et de la Technologie Houari Boumediene, BP 32, El Alia, 16111 Algiers, Algeria

[2] Laboratoire des Matériaux Organiques (LMO), Faculté de Technologie, Université A. MIRA, Route de Targa Ouzemour, 06000 Bejaïa, Algeria

coefficient values calculated using the diffusion model were in the range of 3.8×10^{-10} to 5.8×10^{-10} cm^2/s. Furthermore, the PCL/Ag–MMT films exhibited a strong antibacterial efficiency against *S. aureus*, *E. coli*, *salmonella* and *P. aeruginosa* due to the presence of the long-lasting biocidal silver nanoparticles.

Keywords Active packaging · Poly (ε-caprolactone) · Silver montmorillonite · Silver release · Antimicrobial activity

Introduction

The development and the improvement of materials with the ability to inhibit microbial growth have been of great interest in academic and technological fields due to their potential use in water purification systems, medicinal devices, food packaging and storage, construction and Surface [1–3]. Nowadays, silver nanoparticles filled polymers have been captured attention, from the scientific world, because of their unique electrical, optical, catalytic properties [4–9] and their novelty in being long-lasting biocidal materials with high temperature stability and low volatility [10–12]. The silver nanoparticles can be dispersed inside the polymeric matrix, and/or coated by polymer, thus forming a core–shell structure [13–16]. As an advantage, the resulted material combines the suitable properties of both elements. Meanwhile, studies conducted on AgNPs using different polymers have been reported [17–20]. Conventionally, composites are made by mechanically mixing metal nanoparticles into molten or dissolved polymer matrices. Unfortunately, dispersing nanoparticles homogeneously in a polymer matrix is difficult because of their high surface reactivity [21, 22]. The size, stability, and homogeneity of dispersion of the nanoparticles generally influence the functional performance of the nanocomposites, especially the antibacterial effectiveness [23, 24]. To fully exploit the properties of the silver polymeric nanocomposites, the AgNPs should be as small as possible with a narrow size distribution and without the formation of large aggregates. Nevertheless, a direct incorporation of silver particles in polymers has inherent disadvantages in terms of low water level, gas permeability and heat distortion temperature in case of widespread usage [25]. To obviate these inconveniences, it is recommended to synthesize silver nanoparticles on solid supports to prepare practically applicable supported particles as well as to control the particle size.

Clays [26], zeolites [27, 28] and other aluminosilicates [29, 30] have been used as carriers with good results because of their high ion exchange capacity, high surface and sorptive capacity, negative surface charge, chemical inertness and low or null toxicity [31]. Smectite clays have excellent swelling and adsorption ability, which is especially interesting for the impregnation of antibacterial-active nano-size metals. The metal nanoparticles can be anchored on the external surface of the clay mineral silicate layers or in their interlayer space [32, 33]. Biocompatible and biodegradable polymers have become very important and have gained a lot of attention from both biomedical and ecological quarters in the past decade [34]. Many studies have

confirmed that the antimicrobial agents, when incorporated into the packaging films, could be effective for reducing the amount of organisms in foodstuffs.

In this context, we have used the polycaprolactone (PCL) as the matrix, and montmorillonite (MMT) is used as a dispersant to keep AgNPs in order to develop a new class of PCL/Ag–MMT nanocomposites for active packaging applications. PCL is a semi-crystalline hydrophilic polymer, which is highly biocompatible. It can be processed easily and has high water permeability. These properties have led to the use of PCL in a wide range of applications in medical, cosmetic, food, pharmaceutical etc. [35, 36]. However, the main limitations of PCL, especially in the packaging field, are due to its weak mechanical performances as a result of its low melting point and barrier properties. Many attempts have been made to formulate nanocomposites with PCL to improve its material properties [37–40].

The current work focuses on the elaboration and characterization of antibacterial nanobiocomposite films based on poly (ε-caprolactone) PCL, and different loadings of Algerian silver modified montmorillonite (0, 2, 3, 5 wt% Ag–MMT), prepared by solvent casting process. The main objective of this study is to develop new biodegradable materials with enhanced water barrier, strong antimicrobial activity and slow silver ions release property for active packaging applications. To our knowledge, the fabrication of such materials using PCL as a matrix has not been reported in the literature.

Experimental part

Materials

The clay, used as a solid support for AgNPs, was an Algerian montmorillonite (MMT) extracted from the bentonite category from Roussel in Maghnia (Algeria). It was kindly supplied by ENOF Chemical Ltd, Research Company for non-ferrous matters, Algeria. The montmorillonite (size fraction <2 μm) was extracted from bentonite, using the sedimentation method and then was homoionized with sodium cations (Na–MMT).

All aqueous solutions were prepared with double distilled water (DD-water).

All reagents were of analytical grades and were used as received, that is without further purification.

Poly (ε-caprolactone) (CAPAR650) was supplied by Solvay Chemicals sector-SBU (Belgium). The average number of units in the molar mass was 49,000, with a rate of polydispersity of 1.4.

Preparation of Ag-exchanged montmorillonite

The AgNPs were prepared according to our previous preparation procedure [41].

10 g of Na–MMT was dispersed in 400 mL of DD-water and was vigorously stirred for 1 h. The $AgNO_3$ solution was added into the MMT suspension and the mixture was further vigorously stirred during 24 h at room temperature to obtain the $AgNO_3$/MMT suspension and a completed cation exchange.

A freshly prepared $NaBH_4$ (4×10^{-2} M) solution was then added to the suspension under continuous stirring to reach a constant $AgNO_3/NaBH_4$ molar ratio (1:4). After the addition of the reducing agent to the suspension, the solution turned brown, indicating the formation of AgNPs in the MMT suspension. This latter was then centrifuged at 4200 rpm for 30 min, and the precipitate was washed 4 times, using double distilled water, the aim being to remove the silver ion residue, and then was dried overnight at 40 °C in vacuum overnight.

Preparation of PCL/Ag–MMT nanocomposites

PCL/Ag–MMT composites were prepared at various Ag–MMT contents (2, 3 and 5 % by weight) by solvent casting method, using chloroform as a solvent for PCL and a dispersing medium for Ag–MMT particles. Pure PCL was also prepared in the same way as the composites and was used as a control. Films generated from the different polymeric solutions by solvent evaporation were dried in a vacuum oven for several days at 60 °C.

Characterization

The ATR/FTIR spectra were recorded at room temperature on a Thermo Nicolet Nexus 670 spectrometer with a spectral resolution of 2 cm^{-1} and 60 scans were signal averaged.

The UV–visible spectra of silver modified montmorillonite Ag–MMT and PCL/Ag–MMT biocomposites were recorded over the range of 300–700 nm using the JASCO V-630 Spectrophotometer. The structure and dispersion of the silver-based modified MMT in the PCL matrix were evaluated by wide angle X-ray scattering diffractometer (Philips PW3710 diffractometer), and Transmission Electron Microscope (JEOL 1400 equipped with a MORADA SIS numerical camera at an acceleration voltage of 120 kV).

Differential scanning calorimetry (DSC, TA Instruments DSC Q100) measurements were performed from −80 to 100 °C at 10 °C/min (1st heating), cooled to −80 °C at the same scan rate, then heated again to 100 °C at 10 °C/min (2nd heating). From these scans, glass transition temperature (T_g), melting temperature (T_m) and crystallization temperature (T_c) of the samples were measured. The area under the curve corresponding to the enthalpy was calculated from the instrument software. Thermal scans for each sample were carried out in triplicate and the average values are reported in this study.

Water vapor permeability (WVP)

The water vapor permeations were realized using the ''cups methods'', referring to the standard ISO 7783. The experimental setting consists in a cylindrical vessel filled with a desiccant powder and sealed with the investigated film. For our test, 10 g of $CaCl_2$ was used as the desiccant powder, while the temperature was set to 23 ± 1 °C with a relative humidity of 48 ± 2 %. This method consists of monitoring the water mass uptake of the desiccant powder with time. The water

vapor transmission rate (WVTR) is then calculated from the slope of the mass uptake profile versus time as soon as the steady state is reached using Eq. (1) [42]:

$$\mathrm{WVP} = \frac{\mathrm{WVTR} \times e}{\Delta P}, \tag{1}$$

where WVP is the water vapor permeability coefficient, WVTR is the water vapor transmission rate, e is the film thickness and ΔP is the water vapor partial pressure difference. From the experimental conditions, the water vapor ΔP is 1400.3 Pa calculated for a temperature of 23 °C and a relative humidity of 48 %. Four films of each sample were tested and the results are arithmetically averaged.

Tensile measurements

Tests specimens for tensile measurements were prepared from 1 mm thick plates. The tensile modulus, strength and elongation at break were measured in a Tensile Zwick/Roell Z 100 tester, at a strain rate of 200 mm min^{-1}. The films were conditioned in a desiccator under 50 % RH, at 25 °C, for 48 h before being characterized. The values of tensile strength and elongation at break were obtained basing on the average tensile results of at least five tensile specimens and the results were provided with mean ± SD (standard deviation) values.

Silver ion release tests

The silver ions release was obtained under experimental conditions imitating the physiological medium for 30 days. The concentration of silver in the solution withdrawn from the test medium at the fixed time intervals was determined using Perkin Elmer AAnalyst 700 atomic absorption spectroscopy (AAS). The PCL/Ag–MMT films were cut into two rectangular strips of a 10 cm^2 total area of each film approximately. 5 ml aliquot of HNO_3(2.10^{-3} M) was added to each tube and mixed at 80 rpm at room temperature for time intervals ranging from 1 to 30 days. Three films of each sample were tested.

Evaluation of antibacterial activity

The antibacterial performance of PCL/Ag–MMT composite films against *Staphylococcus aureus* CIP 4.83 (Gram positive) and *Escherichia coli* CIP 53.126, *Salmonella enteric* CIP 80.39 and *Pseudomonas aeruginosa* CIP 82.118 (Gram negative) was assessed by counting the number of bacteria in the sample.

Specimens of 100 mg were introduced in test tubes containing 9 ml of a buffered sodium chloride–peptone solution, pH 7.0. Subsequently, tubes were inoculated with 1 ml of each bacterium. Control experiments with pristine PCL were performed under the same conditions. All samples were incubated in a wrist-action shaker (150 rpm) at 37 °C for 24 h. Afterward, 0.1 ml aliquot from each tube was sown in TSA plates and incubated for 24 h at 37 °C. Finally, viable cells were counted. Three replicate experiments per condition were performed.

Results and discussion

Characterization of the silver-based montmorillonite

Figure 1 shows the ATR/FTIR spectrum of Na–MMT. In the high frequency range, a well defined peak appearing at 3626 cm^{-1} is associated to the stretching mode of the O–H group coordinated to Al cations. The band located at 3442 cm^{-1} is due to the inter-layered O–H stretching (H bonding). Band observed at 1638 cm^{-1} corresponds to H–O–H bending. On the other hand, in the lower frequency range (1300–750 cm^{-1}), the most intense band at 1126, 1032, and 914 cm^{-1} is related to stretching Si–O–Si bond, characteristic of phyllosilicate minerals. Al_2–OH and (Al, Mg)–OH vibration modes are observed at 797 and 778 cm^{-1}, whereas the two strong bands at 523 and 467 cm^{-1} correspond to the bending mode of Si–O and Si–O–M bonds (where M = Mg and Al), respectively [43]. As shown in Fig. 1, there were no many changes in the spectra of Ag–MMT compared with Na–MMT. The shift of the peak at 3442–3435 cm^{-1} in the Ag–MMT spectrum can be associated to the existence of van der Waals interactions between the hydroxyl groups of the MMT layers and the partial positive charge on the surface of AgNPs [44, 45].

The XRD study of Na–MMT and Ag–MMT composites was carried out to determine the location of silver particles on the montmorillonite. From XRD patterns (Fig. 2a), Na–MMT exhibits a sharp peak at $2\theta = 6.4°$ ($d_{001} = 1.38$ nm) corresponding to the (001) basal reflection of MMT. After the silver exchange reaction, no significant shift of the (001) diffraction peak is observed. This means that the d_{001} interlayer distance was not increased and no intercalation of the Ag nanoparticles occurred. Because of their size, the AgNPs could not be located in the

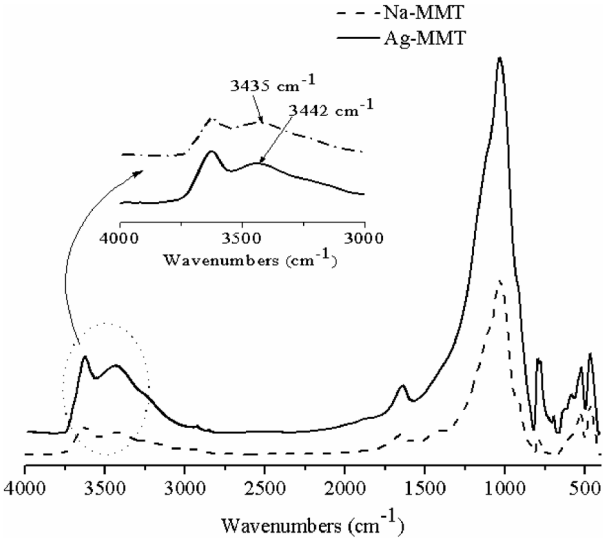

Fig. 1 ATR-FTIR spectra for the Na–MMT and Ag–MMT

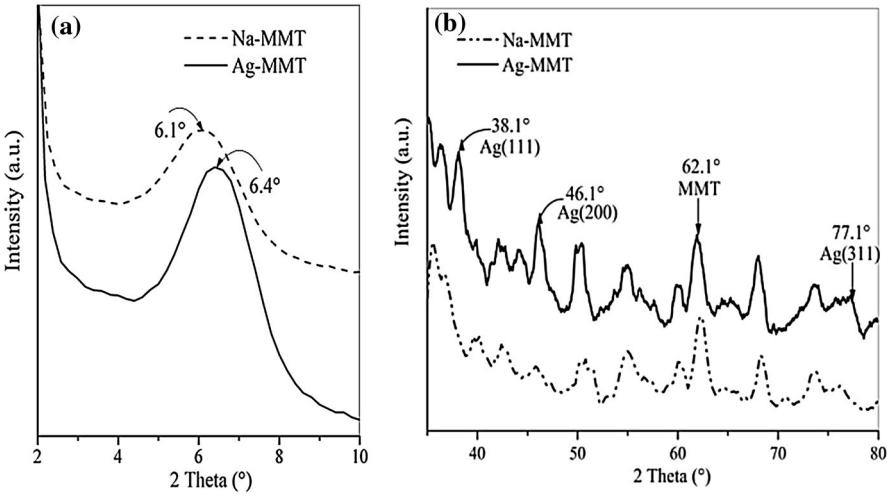

Fig. 2 Wide angle X-ray diffraction patterns (XRD) of unmodified (Na–MMT) and silver modified montmorillonite (Ag–MMT) **a** between 2° and 10° and **b** between 35° and 80°

interlayer space and would be placed on the montmorillonite outer surface. Similar behavior was observed by Petr Praus et al. [46].

The new XRD peaks appearing at 2θ of 38.1°, 46.1°, 64° and 77.1° (Fig. 2b) also confirm the presence of AgNPS in the MMT. They can be attributed to the (111), (200) and (311) silver crystals, respectively **[**47**].** In addition, there is a characteristic peak at about $2\theta = 62.1°$ that characterized to MMT clay (PXRD Ref. No. 00-003-0010) as a stable support. This result confirms the occurrence of silver-modification reaction.

The color of the $AgNO_3$/MMT suspension through the reduction process using $NaBH_4$ changed from colorless to brown reflecting the formation of AgNPs in the MMT suspension. The successful synthesis of Ag nanoparticles colloidal solution was explored by UV–Vis analysis. As it can be seen from Fig. 3, no absorption band is observed in the 300–700 nm range for $AgNO_3$/MMT, indicating that no AgNPs formation has occurred in this sample. After the addition of $NaBH_4$, an intense peak of around 412 nm is detected, reflecting the formation of AgNPs with small diameters [48, 49]. The broadness of the UV–Vis absorption curve states the formation of anisotropic particles, which may be due to broad particle size distribution and agglomeration of the nano-silver particles.

Moreover, TEM analysis provides complementary information on the dispersion and size of silver nanoparticles. From TEM image (Fig. 4), AgNPs can be spotted as dark spherical nanodots of various diameters, which seem unevenly distributed in size and dispersion across the platelets surface of the nanoclay. The spherical particles with a diameter varying between 15 and 20 nm are evenly dispersed on the surface of MMT. It is likely that silver is randomly present across the whole morphology of the Ag–MMT clay.

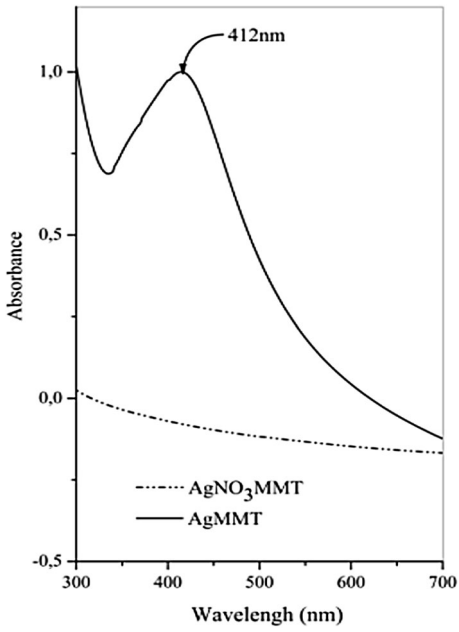

Fig. 3 UV-visible absorption spectra of Ag–MMT and $AgNO_3$-MMT suspensions

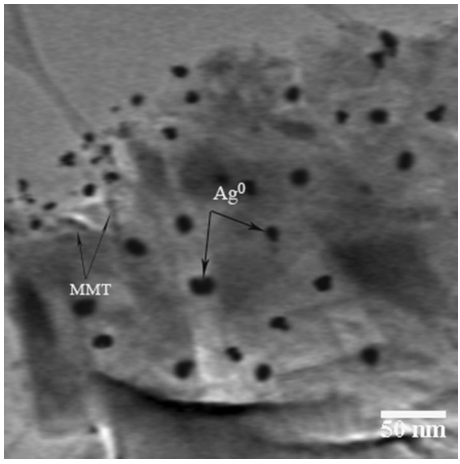

Fig. 4 Typical TEM image of the silver-based nanoclay

The content of silver in the Ag–MMT composite was subsequently determined by AAS after its dissolution in a mixture of HF, HNO3 and HClO4 (5:4:4) [50]. The amount of Ag in Ag–MMT was estimated at 3.2 wt%.

Characterization of the PCL nanobiocomposites

ATR/FTIR spectrum of the neat PCL displays the characteristic absorption bands located at 2945, 2865 and 1723 cm^{-1} corresponding to the stretching vibration of $–CH_2$ and vibration of –C=O bonds, respectively. Figure 5a illustrates ATR/FTIR

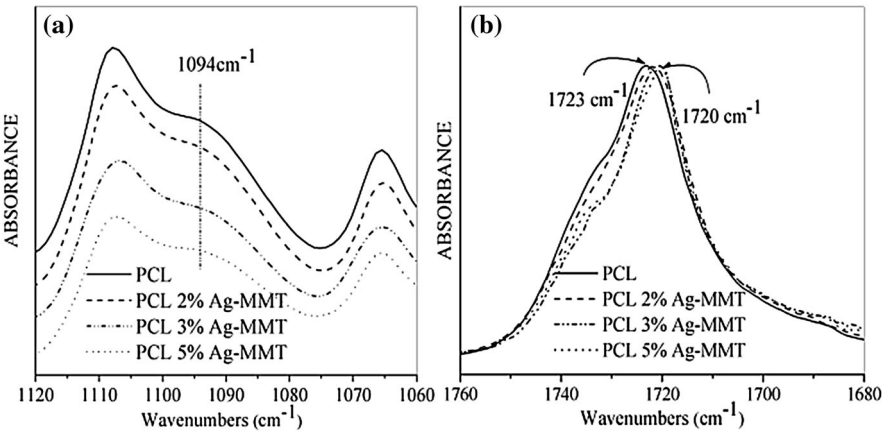

Fig. 5 ATR/FTIR spectra of pristine PCL and its PCL/Ag–MMT nanocomposites **a** in 1120–1060 cm^{-1} region and **b** in 1760–1680 cm^{-1} region

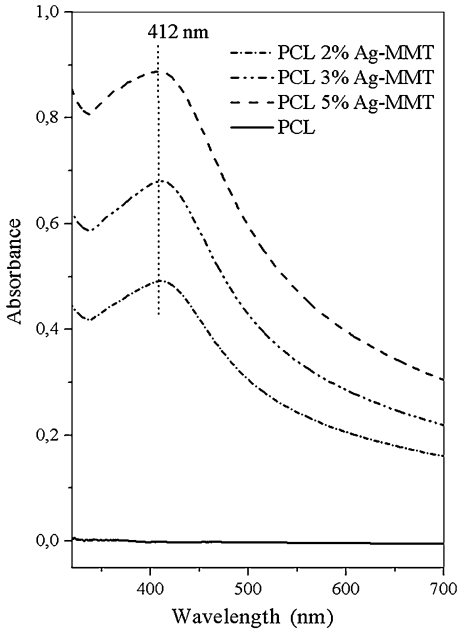

Fig. 6 UV-visible absorption of PCL and its PCL/Ag–MMT nanocomposites

spectra of PCL and its PCL/Ag–MMT nanocomposites in the 1120–1060 cm^{-1} region. As it can be seen from this figure the incorporation of Ag–MMT into the PCL matrix caused a slight difference in shifting and intensity variation for the characteristic bands of PCL. The increase of the shoulder at 1094 cm^{-1} observed in the PCL/Ag–MMT nanocomposites spectra would be related to the silica vibrations. Additionally, the band at 1723 cm^{-1} attributed to the carbonyl stretching of the PCL tends to shift to lower wavenumbers with the Ag–MMT clay content (Fig. 5b). This

change may be induced by specific interactions between the carbonyl groups of PCL and the silver modified clay groups owing to their compatibility [51].

Figure 6 illustrates the UV–visible absorption spectra of pristine PCL and its PCL/Ag–MMT composites. Neat PCL did not show any absorption peak, whereas its PCL/Ag–MMT nanocomposites exhibited a high intensity peak at 412 nm confirming the existence of small AgNPs inside the PCL matrix. In addition, the absorbance intensity of AgNPs increased with increasing Ag–MMT amount into PCL matrix.

The XRD patterns of pristine PCL and its nanocomposites with various Ag–MMT contents are shown in Fig. 7. PCL pattern is characterized by two peaks approximately at $2\theta = 21°$ and 23° corresponding to the (110) and (200) planes, respectively [52], revealing the crystalline structure of PCL. As this figure points out, the crystalline structure of PCL hybrid materials does not change after adding Ag–MMT clay; nevertheless, the characteristic peaks became narrower and their intensities increased with Ag–MMT amount, which indicates an enhancement of the crystallinity of PCL nanocomposites.

The most significant features are encountered in the lower angle range, which gives indication of the clay dispersion. Ag–MMT XRD patterns showed a reflection at about 6.3°. However, the XRD patterns of PCL 2 % Ag–MMT, PCL 3 % Ag–MMT and PCL 5 % Ag–MMT composite hybrids (Fig. 7a) exhibited an absence of the clay basal reflection revealing the formation of mainly exfoliated nanocomposites.

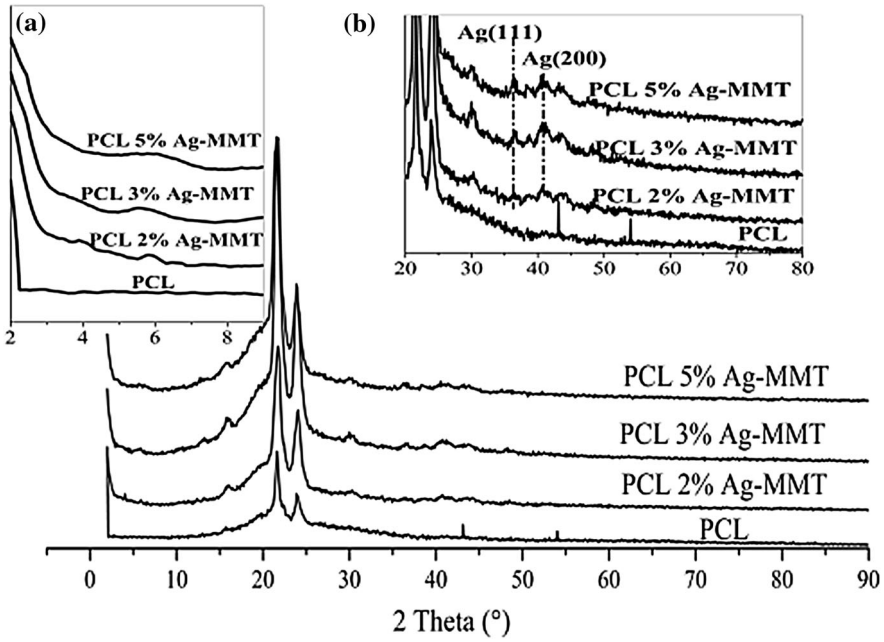

Fig. 7 XRD patterns of PCL, PCL 2 % Ag–MMT, PCL 3 % Ag–MMT and PCL 5 % Ag–MMT nanocomposites

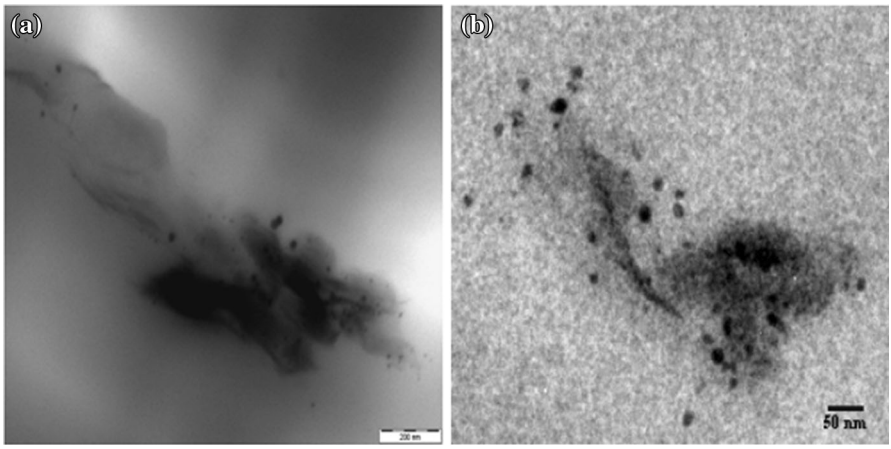

Fig. 8 TEM images of PCL 5 % Ag–MMT nanocomposite **a** at 200 nm *scale bar* and **b** at 50 nm scale bar

In agreement with FTIR studies, the nanocomposite formation may be mainly controlled by hydrogen interactions between the –OH group of the clay and the carbonyl of PCL. This leads to an increase in the gallery spacing allowing the polymer chains to enter and break the galleries during compounding, leading to an exfoliated and an improved dispersion of the clay. The peaks of silver particles are enlarged with increasing the content of Ag nanoparticles (Fig. 7b). These peaks are corresponding to the (111) and (200) planes of the silver nanocrystals with cubic symmetry. XRD results revealed that the MMT layers were predominantly exfoliated and the spherical Ag nanoparticles were randomly distributed in the polymer matrix [53].

The dispersion of Ag–MMT into the different PCL/Ag–MMT (2, 3 and 5 % by weight) matrices was examined by TEM analysis. As an example, Fig. 8 depicts a TEM micrograph of PCL 5 % Ag–MMT nanocomposites. The formation of mainly exfoliated nanocomposite structure was evidenced at high magnification (200 nm scale bar) by the presence of stacked layers randomly dispersed in the PCL matrix. Some individual exfoliated silicate sheets are also shown, as well as the AgNPs are randomly dispersed into the polymer matrix. In size, the particles range from 12 to 25 nm with a mean diameter 14 nm which is in accordance with the UV results.

DSC analysis

DSC analysis was carried out to investigate the Ag–MMT effect on the PCL thermal properties (T_g, T_m and χ). Figure 9 shows DSC thermograms of PCL and its nanocomposite films. Besides the glass transition temperature (T_g) at −65.5 °C, the neat PCL presents an endothermic peak around 59 °C, which is ascribed to the melting temperature (T_m) owing to its semi-crystalline structure.

In nanocomposites curves (Fig. 9a), T_g and T_m values are not markedly affected by Ag–MMT loading. However, the melt crystallization temperature T_c increased

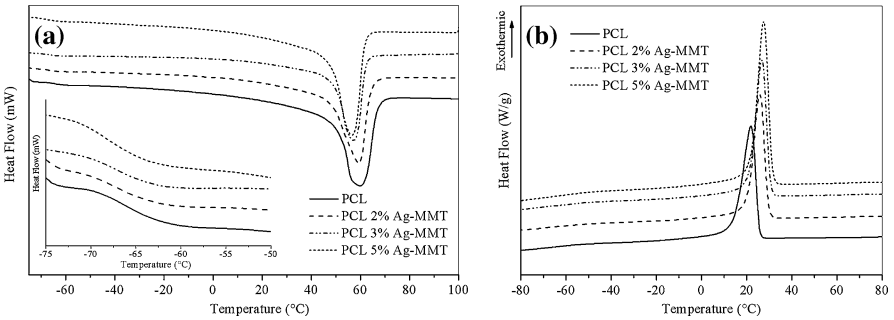

Fig. 9 DSC curves of neat PCL and its PCL/Ag–MMT nanocomposites **a** 2nd heating scan and **b** cooling scan

Table 1 DSC and WVP results of PCL and its PCL/Ag–MMT nanocomposites

Samples	T_g (°C)	T_m (°C)	T_C (°C)	χ (%)	WVP (g/m 24 h atm)
PCL	−65.5 ± 0.3	59.1 ± 0.4	21.7 ± 0.4	38.0 ± 1.1	0.35 ± 0.07
PCL 2 %Ag–MMT	−65.8 ± 0.2	58.3 ± 0.5	25.9 ± 0.3	40.2 ± 1.4	0.18 ± 0.02
PCL 3 %Ag–MMT	−66.1 ± 0.2	57.3 ± 0.2	26.2 ± 0.5	44.5 ± 1.8	0.16 ± 0.04
PCL 5 %Ag–MMT	−67.5 ± 0.4	56.7 ± 0.2	27.0 ± 0.6	45.8 ± 2.1	0.14 ± 0.05

Values are reported as mean ± standard deviation

with the nanofiller loading (Fig. 9b). This increase is attributed to the incorporation of effective nucleation agent Ag–MMT and its satisfactory dispersion in the PCL matrix. Similar results were reported by Yingwei et al. [54], where the authors observed that the addition of a small amount of cloisite 30B to the PCL matrix leads to in an increase of the polymer matrix T_c value.

The crystallinity degree χ (%) was then calculated under the assumption that the heat of fusion is proportional to the crystalline content, as shown in Eq. (2):

$$\chi\,(\%) = \frac{\Delta H_m}{(1 - W_{Ag-MMT})\Delta H_m^{\circ}}, \tag{2}$$

where ΔH_m is the enthalpy of fusion of the sample, ΔH°_m is the enthalpy of fusion of completely crystalline sample and taken in this work as 139 J/g [55] and W_{Ag-MMT} is the weight fraction of Ag–MMT in the nanocomposite. The results are gathered in Table 1.

From Table 1, it can be noticed that the crystallinity degree χ of PCL increases when Ag–MMT is added [54].

Water vapor permeability

Table 1 shows the water permeability values measured for the films as a function of Ag–MMT content. As it can be seen, all composites reduced water vapor

permeability, reflecting the barrier effect of the nanoclay, due to its good dispersion into the PCL matrix, as already discussed in XRD analysis part, leading to a greater tortuosity for water vapor to pass through the film. The WVP values decrease by about 48 % for PCL 2 %Ag–MMT, 54 % for PCL 3 %Ag–MMT and 60 % for PCL 5 %Ag–MMT. Several authors have shown that the diffusion of water vapor is slowed in the presence of nanofillers [56–58]. It is well known that the permeability depends not only on the clay dispersion, but also on the polymer crystallinity. As already revealed by DSC analysis, Ag–MMT acted as a nucleating agent and increased the rate of the crystallites formation. The decrease of WVP values in PCL/Ag–MMT can also be attributed to the higher number of crystallites in the nanocomposites, leading to a high tortuosity.

Mechanical properties

Tensile properties of the PCL/Ag–MMT nanocomposites were studied and data (tensile modulus, tensile strength at break, and percent elongation at break) are summarized in Table 2. Compared to pure PCL, PCL/Ag–MMT nanocomposites have higher mechanical properties. The tensile modulus and the tensile strength were significantly increased by the presence of Ag–MMT clay into PCL matrix. For instance, the addition of 5 wt % of Ag–MMT to the PCL matrix yields to an increase of the tensile modulus by 23 % and the tensile strength by 32 % with respect to the virgin PCL. This result may be related to the good clay dispersion within the polymer matrix. These findings are well correlated with the XRD analysis and TEM micrographs, evidencing an exfoliation of Ag–MMT into PCL matrix.

Silver ion migration

It has been shown [59, 60] that elemental silver particles can provide a large reservoir of antimicrobial silver ions, because in contact with water and dissolved oxygen ($O_{2\ (aq.)}$), they release small amounts of silver ions [61] according to the following Eq. (3).

$$O_{2\,(aq)} + 4H_3O^+ + 4Ag_{(s)} \rightarrow 4Ag^+ + 6H_2O. \quad (3)$$

Hence, polymer materials filled with elemental silver should well be suitable as long-term antimicrobials.

Table 2 Tensile tests results of the pure PCL and its PCL/Ag–MMT nanocomposites

Sample	Modulus, E (MPa)	Strength, σ (MPa)	Elongation at break, ε (%)
PCL	390.0 ± 2.6	27.5 ± 0.6	360.2 ± 38.1
PCL 2 % Ag–MMT	409.0 ± 3.8	31.2 ± 0.7	326.5 ± 18.6
PCL 3 % Ag–MMT	425.0 ± 4.7	34.4 ± 0.5	318.3 ± 21.5
PCL 5 % Ag–MMT	478.6 ± 5.1	36.3 ± 0.8	295.7 ± 23.1

Each value is the mean of five replicates with the standard deviation

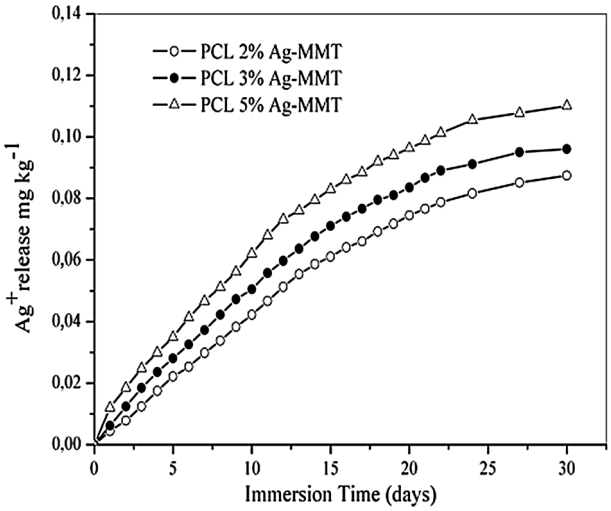

Fig. 10 Silver ions release versus time from PCL nanocomposites containing 2, 3 and 5 % of Ag–MMT

In our study, the silver ions released from the PCL/AgMMT nanobiocomposite films were investigated in a slightly acidified water medium. The measurements were performed with analytes collected after 30 days of storage of the studied materials in water. Figure 10 illustrates the silver ions release versus time from the PCL nanocomposites at different Ag–MMT contents. The results showed that the silver ions that migrated from the nanocomposites into the slightly acidified water medium were less than level of cytotoxicity (10 mg kg^{-1}) over 30 days in all cases with regard to the cytotoxicity level of silver ion for human cells [62].

From Fig. 10, it can be seen that the absolute amount of silver ions released increases gradually and in a non-linear way with the soaking time, indicating that Ag^{+} is released in a controllable way from all PCL/Ag–MMT nanocomposites. It should also be noted that increasing the Ag–MMT amount in the nanocomposites caused a significant increase in silver ion release. The highest silver concentration was found for the PCL 5 % Ag–MMT nanocomposite. Our findings are in good agreement with those published by Damm [62] and Kwakye-Awuah [63].

Analysis of kinetic data

Previous studies [62, 64–66] reported that the mechanism of silver migration from the nanocomposite is generally performed in three main steps: It initially involves water diffusion into polymer, that is, water reacts with silver nanoparticles to produce silver ions, which are subsequently released from the nanocomposite. In this last step, the silver ion release will be governed by diffusion process because most of the silver ions must move from the interior of the specimen to the surface to be released [62, 66].

Figure 10 indicates two different release rate periods. Furthermore, the constant release rate period (straight line) is around 12 days for which the release of silver is

mainly governed by mass transfer in the media (water). This part of the process can be due to the release of the silver which is readily available at the interface polymer/media. In the second part of curve, the release of silver decreases with increasing immersion time due to the increasing mass transfer resistances and the depletion of the silver in the PCL/Ag–MMT nanocomposites.

For the kinetic description of the silver ion release from PCL/AgMMT nanocomposites, the diffusion model was applied in this work. In this model we assume that the stage controlling process was the diffusion. It was simulated the silver ion release process using a model based on Fick's law in unsteady state for one-dimensional plane slab geometry.

The Diffusion model presented by Crank [67] is represented by:

$$\frac{C_t}{C_0} = \frac{4}{\pi^2}\sum_{n=1}^{\infty}\frac{1}{n^2}\exp\left(-\frac{n^2\pi^2 Dt}{l^2}\right), \tag{4}$$

where C_t is silver ion concentration released at time t, C_0 is silver ion concentration at infinity, t is the immersion time (s), D is the apparent diffusivity coefficient (m^2/s), l the thickness of the plate (m), and n is a positive integer.

At short times, Eq. 4 converges very slowly and for $C_t/C_0 < 0.6$ the expression is reduced to.

$$\frac{C_t}{C_0} = \frac{4}{\sqrt{\pi}}\left(\frac{Dt}{l^2}\right)^{1/2}. \tag{5}$$

In this equation, the apparent diffusivity coefficient (D) is the adjustable parameter.

The initial silver ion concentration of the Ag^+ released from the PCL/Ag–MMT nanocomposites is supposed to be equal to the asymptotical value obtained from the silver ions release versus time curve for each PCL/Ag–MMT nanocomposite (Fig. 10).

To evaluate the goodness of model fit, the average absolute deviation (AAD) is used and defined by:

$$\text{AAD}\ (\%) = \frac{100}{n}\sum_{i=1}^{n}\left|\frac{Y_i - Y_{\text{cal};i}}{Y_i}\right|, \tag{6}$$

where n is the number of experimental points, $y_i = C_t/C_0$ is yield determined by experimental point i, and $y_{\text{mod},i}$ is the yield obtained by the model in point i.

Figure 11 illustrates the kinetic modeling of silver ions transfer from PCL/Ag–MMT nanocomposites. The diffusion model showed higher deviations at the beginning of the process between experimental and modeled data, because: (1) the model does not take into account the external mass transfer, (2) an assumption of the slab shape of PCL/AgMMT nanobiocomposite films was applied in this model; however, the polymer can have different geometries. Thus, the representative size of the PCL/AgMMT nanobiocomposite is overestimated. The advantage of this model is to derive information about the apparent diffusivity.

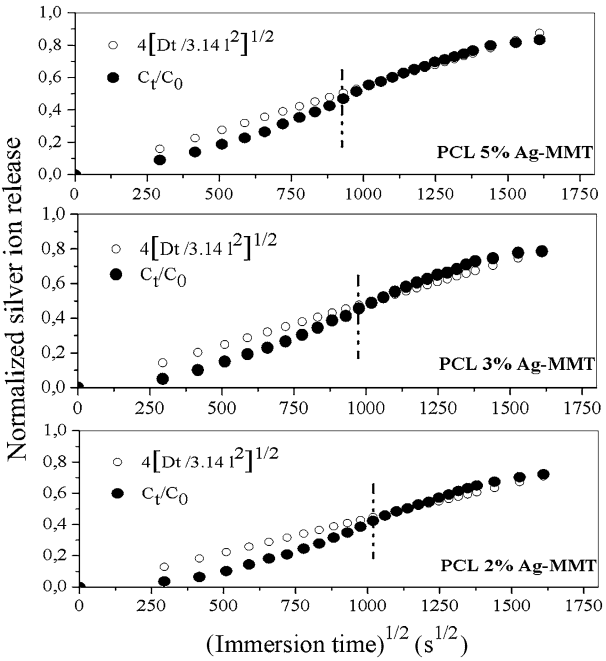

Fig. 11 Silver ion release from PCL/Ag–MMT nanocomposite normalized to the total amount of silver in the polymer as a function of the square root of the immersion time

Before 12 days, it can notice that the silver ion release is dominated by the dissolution of silver particles at the surface of the specimens. However, with increasing of the immersion time (beyond 12 days), the model fitted well the experimental data and the lowest deviation between experimental and correlated data was obtained with the PCL 5 % Ag–MMT nanocomposite. Qualitative assessment of kinetic curves together with their modeling revealed that the release process was mainly limited by the diffusion. Thus, the silver ion must move from the interior of the specimen to the surface to be released.

The resulting apparent diffusivity coefficients of silver ions from the PCL/Ag–MMT nanocomposites summarized in Table 3 have the same order of magnitude that those calculated for other polymer/silver nanocomposites [63, 65].

As expected, the apparent diffusivity coefficient (D) of the silver ions from the nanocomposites was increased by increasing the silver content. The results showed that the diffusion coefficients varied from 3.8×10^{-10} m^2/s to 5.8×10^{-10} cm^2/s which are 5 orders of magnitude, smaller than diffusion coefficient silver in water. The diffusion coefficient of silver in the water was reported 1.77×10^{-5} cm^2/s [62]. It is obvious that the diffusion process in the examined nanocomposites was much slower than in the water.

Table 3 Apparent diffusivity coefficients of silver ions from PCL/Ag–MMT nanocomposites

Sample	$D \times 10^{10}$ (cm^2/s)	AAD (%)
PCL 2 % Ag–MMT	3.8	14.17
PCL 3 % Ag–MMT	4.7	10.10
PCL 5 % Ag–MMT	5.8	7.23

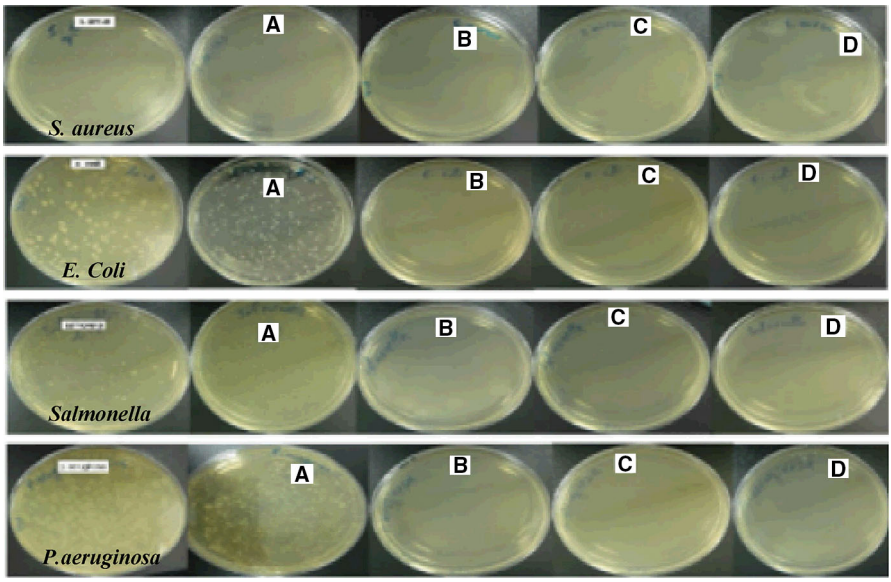

Fig. 12 Growth of the different bacteria in the presence of PCL and its PCL/Ag–MMT nanocomposites

Antimicrobial performance of silver ions as released from the films

To check the antimicrobial performance of the released silver ions, tests of antimicrobial efficacy of the PCL/Ag–MMT materials against *S. aureus* (Gram positive) and *E. coli*, *Salmonella* and *P. aeruginosa* (Gram negative) were investigated and the obtained results are illustrated in Fig. 12.

The antibacterial performance of PCL/Ag–MMT composite films was assessed using the viable cell-counting method. The results were expressed as CFU/ml and the percent reduction was calculated basing on the decrease of final counts from appropriate untreated controls (Table 4).

As shown in the neat PCL and control sample, the concentration of bacteria in the suspension remains nearly unchanged after 24 h. It means that the bacteria survive in the suspension under the conditions. However, in the suspensions which had been in contact with the PCL/Ag–MMT nanocomposites for 24 h, no bacteria could be detected regardless of its strain, which means that most of initial bacteria were dead. Generally, silver in its metallic state can react with moisture to be ionized, releasing of highly reactive Ag^+ ions. The ionized silver can bind itself to proteins causing

Table 4 Growth of *S. aureus*, *E. coli*, *Salmonella* and P. *aeruginosa* in the presence of PCL and its PCL/Ag–MMT nanocomposites

	S. aureus (CFU/ml)	*E. coli* (CFU/ml)	*Salmonella* (CFU/ml)	*P. aeruginosa* (CFU/ml)
Control(Strain)	$(3.2 \pm 0.4) \times 10^9$	$(1.2 \pm 0.2) \times 10^9$	$(3.5 \pm 0.3) \times 10^8$	$(4.4 \pm 0.2) \times 10^8$
PCL	$(3.4 \pm 0.3) \times 10^9$	$(2.2 \pm 0.4) \times 10^9$	$(4.8 \pm 0.6) \times 10^8$	$(5.1 \pm 0.4) \times 10^8$
PCL2 % Ag–MMT	0	0	0	0
PCL3 % Ag–MMT	0	0	0	0
PCL5 % Ag–MMT	0	0	0	0

Each value is the mean of three replicates with the standard deviation

structural changes in the cell wall and also in the nuclear membranes provoking cell death. Indeed, silver ions form complexes with the sulfur-, nitrogen- or oxygen-containing functional groups of bacterial enzymes. This leads to a destabilization of the bacterial cell wall as well as to a disturbance of the metabolism. In addition, silver ions interact with the bacterial DNA preventing the reproduction of the cells [68, 69].

Conclusion

Antimicrobial PCL-based nanobiocomposites for active packaging use were successfully prepared by solvent casting process of the poly (ε-caprolactone) and silver exchanged montmorillonite. PCL/AgMMT nanomaterials have displayed mainly exfoliated structures, wherein the AgNPs with mean diameter of 14 nm were randomly dispersed. Water vapor permeability analysis underlined that the AgMMT addition in PCL promoted a significant decrease reflecting its barrier effect, while DSC investigations showed increased values of crystallinity in the nanocomposites, highlighting the positive influence of the clay on the nucleation process. Tensile results also exhibited an improvement of mechanical properties for the PCL/Ag–MMT nanocomposites compared to those of the pristine PCL. The potential of the silver ion release from the PCL/Ag–MMT films was estimated after immersion in water for several periods of time. The results showed that the silver ions migration from the nanocomposites can be regarded as not only a surface phenomenon but also by a diffusion process in which the silver entities must move from the interior of the specimen to the surface to be released. The antibacterial performance of PCL/Ag–MMT composite films against *S. aureus*, *E. coli*, salmonella and *P. aeruginosa* exhibited a complete growth inhibition of bacteria due to the presence of the long-lasting biocidal silver nanoparticles.

Acknowledgments The authors are grateful to the microbiology laboratory of LABORATOIRIES MERINAL SARL in Algeria for provision of the research facilities.

References

1. Gordon T, Perlstein B, Houbara O, Felner I, Banin E, Margel S (2011) Synthesis and characterization of zinc/iron oxide composite nanoparticles and their antibacterial properties. Colloids Surf A Physicochem 374:1–8 **(Eng aspects)**
2. Deverre E, Purchase D (2007) Effectiveness of domestic antibacterial products in decontaminating food contact surfaces. Food Microbiol 24:425–430
3. Gilbert P, McBain AJ (2001) Biocide usage in the domestic setting and concern about antibacterial and antibiotic resistance. J Infect 43:85–91
4. Liu CJ, Burghaus U, Besenbacher F, Wang ZL (2010) Preparation and characterization of nanomaterials for sustainable energy production. ACS Nano 4:5517–5526
5. Tricoli A, Pratsinis SE (2010) Dispersed nanoelectrode devices. Nat Nanotechnol 5:54–60
6. Chen S, Parker G, Zou G, Su W, Zhang Q (2010) β-Cyclodextrin-functionalized silver nanoparticles for the naked eye detection of aromatic isomers. ACS Nano 4:6387–6394
7. Zeng Q, Jiang X, Yu A, Lu G (2007) Growth mechanisms of silver nanoparticles: a molecular dynamics study. Nanotechnology. 18:035708
8. Severin N, Kirstein S, Sokolov SM, Rabe JP (2009) Rapid trench channeling of graphenes with catalytic silver nanoparticles. Nano Lett 9:457–461
9. Signori AM, Santos KDO, Eising RB, Albuquerque L, Giacomelli FC, Domingos JB (2010) Formation of catalytic silver nanoparticles supported on branched polyethyleneimine derivatives. Langmuir 26:17772–17779
10. Kvitek L, Panacek A, Soukopova J, Kolar M, Vecerova R, Prucek R, Holecova M, Zboril R (2008) Effect of surfactants and polymers on stability and antibacterial activity of silver nanoparticles (NPs). J Phys Chem C 112:5825–5834
11. Pal S, Kyung Y, Myong S (2007) Antibacterial activity and mechanism of action of the silver ion in *Staphylococcus aureus* and *Escherichia coli*. J Appl Environ Microbiol. 73:1712–1720
12. Kumar R, Munstedt H (2005) Silver ion release from antimicrobial polyamide/silver composites. Biomaterials 26:2081–2088
13. Vestal CR, Zhang ZJ (2003) Effects of surface coordination chemistry on the magnetic properties of $MnFe_2O_4$ spinel ferrite nanoparticles. J Am Chem Soc 125:9828–9833
14. Levin CS, Hoffman C, Ali TA, Kelly AT, Morosan E, Nordlander P, Whitmire KH, Halas NJ (2009) Magnetic-plasmonic core-shell nanoparticles. ACS Nano 3:1379–1388
15. Li L, Feng Y, Li Y, Zhao W, Shi J (2009) Fe_3O_4 core/layered double hydroxide shell nanocomposite: versatile magnetic matrix for anionic functional materials. Angew Chem Int Ed 48:5888–5892
16. Li Z, Fredin LA, Tewari P, DiBenedetto SA, Lanagan MT, Ratner MA, Marks TJ (2010) In situ catalytic encapsulation of core-shell nanoparticles having variable shell thickness: dielectric and energy storage properties of high-permittivity metal oxide nanocomposites. Chem Mater 2:5154–5164
17. Zheng M, Gu M, Jin Y, Jin G (2001) Optical properties of silver-dispersed PVP thin film. Mater Res Bull 36:853–859
18. Khanna PK, Singh N, Charan S, Subbarao VVVS, Gokhale R, Mulik UP (2005) Synthesis and characterization of Ag/PVA nanocomposites by chemical reduction method. Mater Chem Phys 93:117–121
19. Lu HW, Liu SH, Wang XL, Qian XF, Yin J, Zhu ZK (2003) Silver nanocrystals by hyperbranched polyurethane assisted photochemical reduction of Ag^+. Mater Chem Phys 81:104–107
20. Zhang Z, Zhang L, Wang S, Chen W, Lei Y (2001) A convenient route to polyacrylonitrile/silver nanoparticle composite by simultaneous polymerization–reduction approach. Polymer 42:8315–8318
21. Dirix Y, Bastiaansen C, Caseri W, Smith P (1999) Preparation, structure and properties of uniaxially oriented polyethylene-silver nanocomposites. J Mater Sci 34:3859–3866
22. Ghosh K, Maiti SN (1996) Mechanical properties of silver-powder-filled polypropylene composites. J Appl Polym Sci 3:323–331
23. Lok CN, Ho CM, Chen R, He QY, Yu WY, Sun H, Tam PK, Chiu JF, Che CM (2007) Silver nanoparticles: partial oxidation and antibacterial activities. Biol Inorg Chem. 12:527–534
24. Jiang W, Kim BY, Rutka JT, Chan WC (2008) Nanoparticle-mediated cellular response is size dependent. Nat Nanotechnol 3:145–150
25. Bordes P, Pollet E, Averous L (2009) Nano-biocomposites: biodegradable polyester/nanoclay systems. Prog Polym Sci 34:125–155

26. Zhao D, Zhou J, Liu N (2006) Preparation and characterization of Mingguang palygorskite supported with silver and copper for antibacterial behavior. Appl Clay Sci 33:161–170
27. Top A, Ulku S (2004) Silver, zinc, and copper exchange in a Na-clinoptilolite and resulting effect on antibacterial activity. Appl Clay Sci 27:13–19
28. Rivera-Garza M, Olguın MT, Garcia-Sosa I, Alcantara D, Rodriguez-Fuentes G (2000) Silver supported on natural Mexican zeolite as an antibacterial material. Microporous Mesoporous Mater. 39:431–444
29. Dizman B, Badger JC, Elasri MO, Mathias LJ (2007) Antibacterial fluoromicas: a novel delivery medium. Appl Clay Sci 38:57
30. Li B, Yu S, Hwang JY, Shi S (2002) Antibacterial vermiculite nano-material. J Miner Mater Charact Eng 1:61–68
31. Carretero MI (2002) Clay minerals and their beneficial effects upon human health. A review. Appl Clay Sci. 21:155–163
32. Rasal RM, Janorkar AV, Hirt DE (2010) Poly(lactic acid) modifications. Prog Polym Sci 35:338–356
33. Papp S, Szücs A, Dekany I (2001) Preparation of Pd nanoparticles stabilized by polymers and layered silicate. Appl Clay Sci 19:155–172
34. Ikada Y, Tsuji H (2000) Biodegradable polyesters for medical and ecological applications. Macromol Rapid Commun. 2:117–132
35. Khatiwala VK, Shekhar N, Aggarwal S, Mandal UK (2008) Biodegradation of poly(ε-caprolactone) (PCL) film by Alcaligenes faecalis. J Polym Environ 16:61–67
36. Lei Y, Rai B, Ho KH, Teoh SH (2007) Bioactive polycaprolactone 20 % tricalcium phosphate composite scaffolds for bone engineering. Mater Sci Eng C 27:293–298
37. Yahiaoui F, Benhacine F, Harrar-Ferfera H, Habi A, Hadj-Hamou AS, Grohens Y (2015) Development of antimicrobial PCL/nanoclay nanocomposite films with enhanced mechanical and water vapor barrier properties for packaging applications. Polym Bull 72:235–254
38. Chen B, Evans JRG (2006) Poly(ε-caprolactone)-clay nanocomposites: structure and mechanical properties. Macromolecules 39:747–754
39. Lepoittevin B, Devalckenaere M, Pantoustier N, Alexandre M, Kubies D, Calberg C, Jerome R, Dubois P (2002) Poly(ε-caprolactone)/clay nanocomposites prepared by melt intercalation: mechanical, thermal and rheological properties. Polymer 43:4017–4023
40. Ludueña LN, Alvarez VA, Vazquez A (2007) Viscoelastic behavior of polycaprolactone/clay nanocomposites. Mater Sci Eng A 460:121–129
41. Benhacine F, Hadj-Hamou AS, Habi A, Grohens Y (2015) Development of antimicrobial poly(ε-caprolactone)/poly(lactic acid)/silver exchanged montmorillonite nanoblend films with silver ion release property for active packaging use. Int Polym Proc 30:511–521
42. Corre YM, Bruzaud S, Audic JL, Grohens Y (2012) Morphology and functional properties of commercial polyhydroxyalkanoates: a comprehensive and comparative study. Polym Test 31:226–235
43. Alemda A, Güngör N, Ece OI, Atici OJ (2005) The rheological properties and characterization of bentonite dispersions in the presence of non-ionic polymer PEG. J Mater Sci 40:171–177
44. Gao Y, Choudhury NR, Dutta NK (2010) Systematic study of interfacial interactions between clays and an ionomer. J Appl Polym Sci 117:3395–3405
45. Shameli K, Bin Ahmad M, Yunus WMZW, Ibrahim NA, Gharayebi Y, Sedaghat S (2010) Synthesis of silver/montmorillonite nanocomposites using γ-irradiation. Int J Nanomed 5:1067–1077
46. Praus P, Turicová M, Karlíková M, Kvítek L, Dvorský R (2013) Nanocomposite of montmorillonite and silver nanoparticles: characterization and application in catalytic reduction of 4-nitrophenol. Mater Chem Phys 140:493–498
47. Temgire MK, Joshi SS (2004) Optical and structural studies of silver nanoparticles. Radiat Phys Chem 71:1039–1044
48. Ahmad MB, Shameli K, Darroudi M, Yunus W, Ibrahim A (2009) Synthesis and characterization of silver/clay/chitosan bionanocomposites by UV-irradiation method. Am J Appl Sci 6:2030–2035
49. Aihara N, Torigoe K, Esumi K (1998) Preparation and characterization of gold and silver nanoparticles in layered laponite suspensions. Langmuir 14:4945–4949
50. Praus P, Turicová M, Karlíková M (2009) Preparation of silver-montmorillonite nanocomposites by reduction with formaldehyde and borohydride. J Braz Chem Soc 20:1351–1357
51. Lin WJ, Lu CH (2002) Characterization and permeation of microporous poly(ε-caprolactone) films. J Membr Sci 198:109–118

52. Jiang S, Ji X, An L, Jiang B (2001) Crystallization behavior of PCL in hybrid confined environment. Polymer 42:3901–3907
53. Wu T, Xie T, Yang G (2009) Preparation and characterization of poly (ε-caprolactone)/Na^+-MMT nanocomposites. Appl Clay Sci 45:105–110
54. Yingwei D, Iannace S, Di Maio E, Nicolais L (2003) Nanocomposites by melt intercalation based on polycaprolactone and organoclay. J Polym Sci B Polym Phys 41:670–678
55. Pitt CG, Chaslow FI, Hibionada YM, Klimas DM, Scindler A (1981) Aliphatic polyesters. I. The degradation of poly(ε-caprolactone) in vivo. J Appl Polym Sci 26:3779–3787
56. Park HM, Liang X, Mohanty AK, Misra M, Drzal LT (2004) Effect of compatibilizer on nanostructure of the biodegradable cellulose acetate/organoclay nanocomposites. Macromolecules 37:9076–9082
57. Rhim JW, Lee JH, Kwak HS (2004) Mechanical and barrier properties of soy protein and clay mineral composite films. Food Sci Biotechnol 14:112–116
58. Rhim W, Hong SI, Park HM, Ng PK (2006) Preparation and characterization of chitosan-based nanocomposite films with antimicrobial activity. J Agric Food Chem 54:5814–5822
59. Fortunati E, Peltzer M, Armentano I, Jiménez A, Kenny JM (2013) Combined effects of cellulose nanocrystals and silver nanoparticles on the barrier and migration properties of PLA nano-biocomposites. J Food Eng 118:117–124
60. Fernandez A, Soriano E, Hernández-Muñoz P, Gavara R (2010) Migration of antimicrobial silver from composites of polylactide with silver zeolites. J Food Sci 75:186–193
61. Hoskins JS, Karanfil T, Serkiz SM (2002) Removal and sequestration of iodide using silver-impregnated activated carbon. Environ Sci Technol 36:784–789
62. Damm C, Munstedt H, Rosch A (2008) The antimicrobial efficacy of polyamide6/silver nano and microcomposites. Mater Chem Phys 108:61–66
63. Kwakye-Awuah B, Williams C, Kenward MA, Redecka I (2008) Antimicrobial action and efficiency of silver-loaded zeolite X. J Appl Microbiol 104:1516–1524
64. Radheshkumar C, Münstedt H (2006) Antimicrobial polymers from polypropylene/silver composites-Ag^+ release measured by anode stripping voltammetry. React Funct Polym 66:780–788
65. Jokar M, AbdulRahman R (2014) Study of silver ion migration from melt blended and layered deposited silver polyethylene nanocomposite into food simulants and apple juice. Food Addit Contam Part A 31:734–42
66. Zapata PA, Tamayo L, Páez M, Cerda E, Azócar I, Rabagliati FM (2011) Nanocomposites based on polyethylene and nanosilver particles produced by metallocenic "in situ" polymerization: synthesis, characterization, and antimicrobial behavior. Eur Polym J 47:1541–1549
67. Crank J (1975) The mathematics of diffusion, 2nd edn. Clarendon Press, Oxford
68. Russel AD, Hugo WB (1994) Antimicrobial activity and action of silver. Prog Med Chem 31:351–370
69. Feng QL, Wu J, Chen GQ, Cui FZ, Kim TN, Kim JO (2000) A mechanistic study of the antibacterial effect of silver ions on *Escherichia coli* and *Staphylococcus aureus*. J Biomed Mater Res 52:662–668